Carbohydrate Polymer Technologies and Applications 4 (2022) 100249

Contents lists available at ScienceDirect

Carbohydrate Polymer Technologies and Applications

journal homepage: www.sciencedirect.com/journal/carbohydrate-polymer-technologies-and-applications

Synthesis and characterization of nanofibrilated cellulose films modified with blocked isocyanates in aqueous media and their barrier properties to water vapor and oxygen

Gustavo de Souza [a,b], Mohamed Naceur Belgacem [b], Alessandro Gandini [b], Antonio José Felix Carvalho [a,*]

[a] Department of Materials Engineering, Sao Carlos School of Engineering (EESC), University of São Paulo - USP, 13563-120 São Carlos, SP, Brazil
[b] Université Grenoble Alpes, CNRS, Grenoble INP, LGP2, F-38000, Grenoble, France

ARTICLE INFO

Keywords:
Nanofibrillated cellulose films
Blocked isocyanate emulsion
Blocked isocyanate suspensions
Desmodur AP stabil
Urethane modified nanofibrillated cellulose films
Isocyanate deblocking

ABSTRACT

Hydrophobic nanofibrilated cellulose (NFC) films were prepared by the casting of a mixture of NFC suspension in an aqueous emulsion of two blocked isocyanates - one prepared by the reaction of 4,4′- methylenebis (phenyl isocyanate) and phenol (MDI-2Ph) and a commercial one from trimethylol propane and toluene diisocyanate (Desmodur AP Stabil®) (TMP-TDI-3Ph),). The drying procedure was performed in two steps, i.e., first at 60 °C for 24 h and then at 170 °C for 10 min. Infrared spectroscopy (FT-IR), elemental analysis, and 13 C—NMR confirmed the chemical modification of cellulose. The NFC modified films showed an approximately 40 g m^{-2}.day^{-1} water vapor transmission rate, which is almost 75% lower than that of non-modified NFC films (153 g m^{-2}.day^{-1}). The film modified with TMP-TDI-3Ph showed a very low oxygen transmission rate and lower than that with MDI-2Ph When exposed to a wet environment, the modified films maintained their stiffness with Young's modulus around 5 GPa, whereas that of non- modified films decreased from approximately 6.5 GPa to below 0.1 GPa.

1. Introduction

Short-term materials (e.g., polymeric packaging) have become one of the main current technical issues due to their incorrect disposal in the environment. Biomass-derived polymers such as cellulose are potential candidates to replace several synthetic polymers in packaging, medicine, clothing, and other areas (Klemm et al., 2018; Mahmud et al., 2021; Sugiarto et al., 2022).

Cellulose is a worldwide available polysaccharide derived mainly from wood and annual plants (e.g., sisal, sugar cane bagasse, and hemp), with a production of approximately 7.5 × 10^{10} tons per year (Habibi, 2014).

The emergence of nanofibrilated cellulose (NFC) has opened new opportunities for the use of cellulose in place of conventional plastics in short-time applications such as food packages (Nechyporchuk et al., 2016; Rol et al., 2019). NFC is a promising material due to its low cost, renewable character, biodegradability, and outstanding strength/-weight ratio. Moreover, it is easily functionalized (Gandini & Belgacem, 2016; Ghasemlou et al., 2021; Habibi, 2014) and can be used for the production of several advanced materials (e.g., high-performance nanocomposites (Siqueira et al., 2010) and high-performance all-cellulose films or nanopapers (González et al., 2014; Operamolla, 2019; Sethi et al., 2018, 2019)). NFC films are easily produced by the drying of NFC suspension, which leads to a greater entanglement of the nanofibers, hence, compact, smooth, low porosity, and resistant films with excellent oxygen barrier and potentially good candidates for packaging (J. Wang et al., 2018).

Nonetheless, cellulose inherent hydrophilicity makes NFC films susceptible to moisture, affecting their mechanical properties, dimension stability, and barrier properties to oxygen and water (Lindström & Aulin, 2014; Sehaqui, Zimmermann & Tingaut, 2014).

The methods mostly adopted for reducing the hydrophilicity of NFC films involve chemical modifications that require special conditions (e.g., anhydrous reaction medium and use of complex chemicals (Balu et al., 2008; Forsman et al., 2017; Operamolla, 2019; Sehaqui et al., 2014; Solala et al., 2018).

An interesting approach to overcome those limitations is the use of blocked isocyanates as chemical modifying agents, due to their low

* Corresponding author.
E-mail address: toni@sc.usp.br (A.J.F. Carvalho).

https://doi.org/10.1016/j.carpta.2022.100249

Available online 17 September 2022

toxicity and possibility of use in wet environments (Paquet et al., 2010). They are thermo-reversible addition compounds of isocyanates and hydroxyl compounds; deblocking occurs under heating and generates free isocyanate (Carvalho et al., 2005; Delebecq et al., 2013; Gironès et al., 2007, 2008; Lu et al., 2020; Rol et al., 2019; Wicks & Wicks, 1999; Zhou et al., 2020). Among the blocking agents for isocyanates, phenol is a traditional material due to its low cost and relatively low deblocking temperature (170–180 °C), which is above that of NFC film drying and below the onset of cellulose degradation (Gironès et al., 2007). Although phenol is not recommended for certain uses due to its toxicity, the amount released from the deblocking of isocyanates is very low, since the modification is limited to the surface of the fibers. Nonetheless, other blocking agents can be explored in the future.

This article addresses the preparation of modified nanocellulose films by the casting of a mixture of NFC suspension and an emulsion of blocked isocyanates. Two blocked isocyanates, i.e., a difunctional one prepared by the reaction of 4,4-methylenebis (phenyl isocyanate) (MDI) with phenol (MDI-2Ph) and a polyfunctional commercial material prepared from trimethylol propane (TMP) and toluene diisocyanate (TDI) with trade name Desmodur AP Stabil® (TMP-TDI-3Ph) were used. The casting procedure was followed by a thermal treatment at 170 °C for deblocking and nanofibrilated cellulose modification. The materials were characterized by FT-IR, elemental analysis (EA), ^{1}H and ^{13}C NMR, scanning electron microscopy, atomic force microscopy, mechanical tensile test in dry and wet conditions, tear testing, and barrier to oxygen and water vapor. Films treated with MDI-2Ph and water vapor showed an increase in wet stiffness and barrier properties to water vapor, whereas the barrier to oxygen of the films treated with TMP-TDI-3Ph was significantly enhanced due to the formation of more urethane bonds.

2. Materials and methods

2.1. Chemicals and materials

Nanofibrilated cellulose (NFC) from eucalyptus *(Eucalyptus grandis)* with 3.2% solid content was kindly supplied by Suzano S/A - Brazil. The diameter distribution of the nanofibers was measured by Atomic Force Microscopy (AFM) analysis through the counting of 50 NFC individual fibers, which provided $D_{50} = 23$ nm and $D_{90} = 73$ nm (de Souza et al., 2021). The mean length was estimated as 2–3 μm. Mechanical defibrillation processes are based on the use of an intensive shear milling in which fibers and nanofibers are separated without extensive degradation.

Technical grade 4,4-methylenebis (phenyl isocyanate) (MDI), reagent grade phenol, dibutyltin dilaurate (DBTL), reagent grade dimethyl sulfoxide (DMSO), and dodecyl benzene sulfonic acid (DBSA) were supplied by Sigma–Aldrich-USA and used as received. Zinc octanoate was supplied by Iracema Ltda-Brazil, and reagent grade butyl acetate, xylene, and methylene chloride were supplied by Sigma–Aldrich - USA and dried with 4 Å molecular sieves for at least 72 h before use. The commercial blocked isocyanate composed of trimethylol propane, (2,4/2,6 – 80/20)-toluene diisocyanate, and phenol in 1:3:3 molar proportions was supplied by Bayer under the commercial name of Desmodur AP Stabil®. The reaction path and structure are provided in the supplementary materials (Scheme S1) and a complete list of the chemicals used is shown in Table S1 with NCBI link.

2.2. Blocked diisocyanate preparation

5 g (20 mmol) of MDI and 100 ml of anhydrous butyl acetate were added to a three-neck round bottom flask immersed in water bath at 45 °C at N_2 constant flow and magnetic stirring. 3.76 g (40 mmol) of phenol and 0.1 ml of DBTL diluted in 30 ml of anhydrous butyl acetate at 45° were added dropwise under agitation for 15 min. The agitation was maintained for three hours, thus leading to a white precipitate. The reaction evolution was monitored by free NCO titration with di-n-butylamine (ASTM D-1638–74). The product was a white powder, isolated by evaporation of the solvent at 30 °C in a rotary evaporator under reduced pressure. It was washed twice with 2-propanol and dried at 60 °C for 1 h. Approximately 8 g of the adduct were obtained with a 91% yield of the theoretical value. Scheme S 2 shows the structure of the adduct.

2.3. Emulsion preparation

The emulsions of blocked isocyanates were prepared by the addition of their solution in DMSO directly into the NFC suspension in which a surfactant was dissolved. 350 mg of MDI-2Ph or 310 mg of TMP-TDI-3Ph dissolved in 25 mL of DMSO with 18 mg of zinc octanoate at 50 °C and 120 g of a 1wt% NFC suspension with 16 mg of DBSA were used. The emulsions were homogenized in a T25-Ultra-Turrax IKA operating at 10,000 rpm for five minutes and then sonicated by an UP400S Ultrasonic Processor (Hielscher) (400 Watts) for five minutes with 0.5 s pulses and working at 240 Watts (60% power). The amounts of available NCO per gram of NFC used were 1.330 mmol/g for MDI-2Ph and 0.805 mmol/g for TMP-TDI-3 pH. The latter amount represents an excess; since it is estimated, only 1% of NFC hydroxyls is available on the surface for chemical modification (Gironès et al., 2008).

2.4. Films preparation

Neat NFC films were prepared by pouring 90 g of the NFC suspension degassed in a vacuum desiccator for 10 min into a glass dish plate mold (15 × 10 cm) and dried in an air circular oven for 24 h at 60 °C. Modified NFC was prepared with 120 g of the mixture of NFC/blocked isocyanate. Cast films were then dried in an oven at 170 °C for ten minutes, which led to the production of films of 60 and 80 g/m^2 grammage for neat NFC and modified NFC films, respectively. The films were then washed twice with hot xylene and butyl acetate (75/25 v/v), rinsed several times with methylene chloride for the removal of any residue of reactants, and dried at 60 °C for 1 h. At the end of the process, films of approximately 0.9 g and 46 to 92 μm thickness (Table S3) were obtained.

2.5. Characterization

2.5.1. Fourier transformed infrared spectroscopy - FT-IR and elemental analysis (EA)

FT-IR spectra were collected in the 4000 cm^{-1} to 650 cm^{-1} range with a Perkin-Elmer Spectrum 100 with attenuated total reflectance (ATR). The spectra were normalized with respect to absorption at 896 cm^{-1} peak from C—O-C absorption and an elemental analysis was performed on a Fisons - EA-1108 CHNS from thermoscientific.

2.5.2. ^{1}H—Nuclear magnetic resonance

A ^{1}H nuclear magnetic resonance (NMR) analysis was conducted in a Bruker AVANCE 600 NMR. 200 mg of the sample in 4 mL of deutered dimethyl sulfoxide were used in a 10 mL NMR tube.

2.5.3. Solid-state ^{13}C-nuclear magnetic resonance

^{13}C nuclear magnetic resonance (NMR) analyses were performed in a Bruker AVANCE 600 NMR. The films were pulverized by a longitudinal crio-crushing mill device (RETSCH, Germany) working for 10 min at 30 Hz.

2.5.4. Scanning electron microscopy – SEM

SEM images were acquired in the secondary electrons (SE) mode under an Inspect F-50 (FEI) microscope working at 2.0 kV and with 8.0 mm working distances. Samples were prepared by fixing films onto a double side carbon tape. Stubs were further metalized for 90 s with a platinum target.

2.5.5. Atomic force microscopy – AFM

AFM analyses were performed in an AFM model Flex-Axiom (Nanosurf) in tapping mode by a model Tap190Al-G silicon scanning probe. Film squares of 1 × 1 cm, previously dried at 60 °C for 2 h, were bonded in a double side tape and pressed in the sample holder; images were processed by Gwyddion® software, which also calculated three parameters of roughness set by ASME B46.1–1995, being Ra the average roughness, Rq the square root roughness and Rt the maximum profile height.

2.5.6. UV-VIS

The in-line light transmittance was measured in the 200–1000 nm region by a model UVM51 spectrophotometer from BEL photonics, Italy. The transmittance spectra were acquired using air as background and the transparency or opacity of the films was evaluated by measuring the percent light transmittance at 660 nm (T660), in accordance with(Roy & Rhim, 2020). Three measurements were taken per sample and the value obtained was the mean of light transmittance.

2.5.7. Grammage, density and porosity

Grammage, measured as mass per unit area (g/m^2), were obtained by weighing samples of 50 × 50 mm (0.1 mg readability). A digital micrometer (Adamel Lhomargy 120 mm, France) measured the sample thicknesses, and porosity was calculated by relation (1- ρ_m/ρ_t), where ρ_m is the measured density and ρt is the theoretical cellulose density, taken as 1.5 $g.cm^{-3}$.

2.5.8. Tensile test in dry and wet conditions

Tensile properties were measured by an Instron 3365 universal testing machine equipped with a 5 kN load cell with 0.5 $mm.min^{-1}$extension rate and 25 mm distance between the grips. Five 35 × 5 mm rectangular specimens were used for each sample, and tests were performed at 23 °C and 48% relative humidity. The samples were preconditioned in the same environment for at least 24 h prior to testing. A semi-wet tensile test was performed with the same apparatus in which 10 μl of distilled water were placed in the middle length of the specimen and left to rest for1 min before measurement. The excess water that did not permeate the specimen was dried with absorbing paper and the sample was placed in the testing grips.

2.5.9. Tear test

The tear resistance of the films was measured by a Noviprofibre tear tester (Elmendorf, France) equipped with a 4000 mN pendulum. The precutting notch was 20 mm long and the specimens were cut into 50 × 50 mm^2 squares.

2.5.10. Thermogravimetric analysis – TGA

TGA analyses were conducted on a Pyris (Perkin Elmer, USA) thermogravimetric analyzer operating under 20 mL min^{-1} constant N_2 flow, at 25 to 700 °C, and10 °C min^{-1} heating rate.

2.5.11. Water contact angle – WCA

A KSV - CAM 101 measured the static contact angles and five specimens were cut into rectangular shapes of 5 mm width and 30 mm length from different regions of the films. 40 pictures were taken with 16 ms intervals. Five drops of distilled water (droplet with ~5 μl volume) were deposited for each experiment and measurements were performed at 23 °C and 30% RH.

Contact angle measurements were taken with di-iodomethane for the estimation of the surface tension, and the surface tension (γ_S) of the films was calculated by equations (1), (2), (3) adopting polar and dispersive parts as $\gamma_L^p = 46.4$ mN/m; $\gamma_L^d = 26.4$ mN/m for water and $\gamma_L^p = 0$ mN/m; $\gamma_L^d = 50.8$ mN/m for di-iodomethane (Hubbe et al., 2015).

$$\gamma_L(1+cos\theta) = 2\left(\gamma_L^d\gamma_S^d\right)^{0.5} + 2\left(\gamma_L^p\gamma_S^p\right)^{0.5} \quad (1)$$

$$\gamma_L = \gamma_L^p + \gamma_L^d \quad (2)$$

$$\gamma_S = \gamma_S^p + \gamma_S^d \quad (3)$$

2.5.12. Water vapor absorption test

Water Vapor Absorption tests were performed in accordance with ASTM E-104 (1985). The test samples had been previously dried at 60 °C in a circular oven for 3 days until mass stabilization on the 4th digit scale. Then samples were placed in a desiccator containing a saturated solution of potassium sulfate (K_2SO_4) at 25 °C, which yielded RH = 97.5% relative humidity. Three 2.5 × 2.5 cm specimens were used for each sample; they were weighted after 1 h, 3 h, 5 h, 24 h and then at intervals of 24 h in the first week, 48 h in the second, and 72 h after the second week until saturation. From the mass increase vs time plot the saturation point could be determined.

2.5.13. Water vapor transmission rate – WVTR

WVTR tests were performed according to the ASTM E96 desiccant method. In summary this test consists of using the film sample as a cover for an aluminum pan with a standard open mouth area filled with a certain amount of desiccant salt. The film is fixed on the aluminum device and place inside a chamber with controlled UR. The samples are weighted at regular time intervals and the mass increase vs time curve is built. For the WVTR tests presented here, aluminum testing cups of 3000 mm^2 open mount area were filled with 15 g of calcium chloride desiccant and sealed at the edges. The assemblies were placed in a 50% humidity-controlled environment and the increase in mass due to the water vapor absorption by the salt was measured over time. Equation (2) calculated WVTR $ing.m^{-2}.day^{-1}$ from mass vs time plot, where (G/t) is the angular coefficient in g/h and A is the cup mouth area in m^2.

$$WVTR = \left(\frac{G}{t}\right)\Big/A \quad (4)$$

2.5.14. Oxygen transmission rate - OTR

OTR measurements were obtained by an 8001 Oxygen Permeation Analyser (Systech Illinois, USA) equipped with a coulometric oxygen sensor, according to ASTMF1927–07. Double bonded adhesive aluminum foils of 2.54 cm^2 open area were used for placing the film samples in the measurement device.

2.5.15. Statistical analysis

Variance analysis (ANOVA) and Tukey's multiple comparison test were performed by Minitab® software and statistical analyses for Tensile test, Tear test, and WCA values were conducted with 5% (α = 0.05) significance level.

3. Results and discussion

3.1. Preparation and characterization of blocked isocyanate (MDI-2Ph)

Fig. 1 shows the FTIR spectra of MDI, phenol, and blocked isocyanates. The isocyanate consumption is confirmed by the disappearance of the NCO absorption band at 2262 cm^{-1}. The narrow sharp vibration at 3323 cm^{-1} confirms the presence of -NH due to the formation of urethane bonds and the absorptions at 1720 cm^{-1} and 1590 cm^{-1} are related to C = O and H—NCO from phenyl carbamate (Delebecq et al., 2013; Gironès et al., 2008). Urea was formed by the reaction of free NCO and amines and confirmed by the presence of C = O vibration at 1638 cm^{-1}. The 2920 −2855 cm^{-1} absorption increase for MDI-2Ph with respect to the precursor can be attributed to the formation of disubstituted ureas and allophanates.

Fig. 2(a) displays the ^1H NMR spectra of MDI-2Ph The N—H characteristic absorption from phenyl carbamates is observed at 9.3 ppm (B) and the C—H shifts from the aromatic rings of phenol and MDI

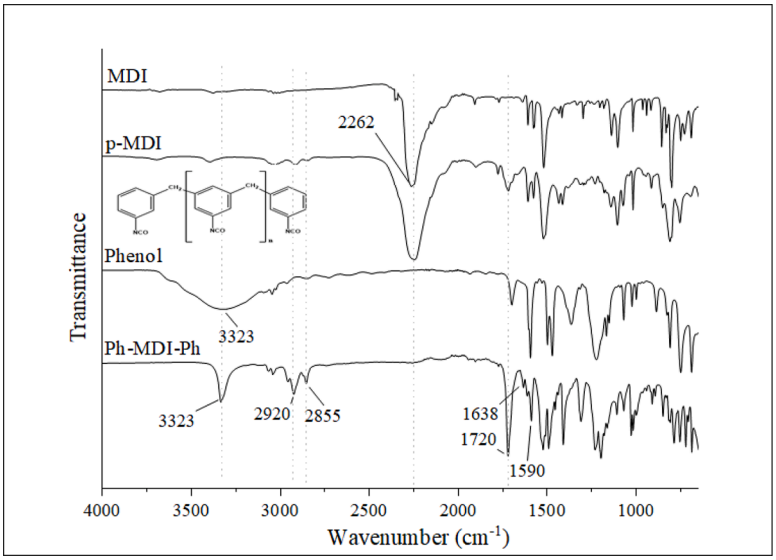

Fig. 1. FT-IR spectra of reactants (MDI and phenol), polymerized MDI (p-MDI), and synthetized adduct (MDI-2Ph).

absorption are observed at 7.4–7.3 ppm (D) and 7.1 ppm (E), respectively. C—H peaks from -CH and -CH_2 of MDI are detected in the 4.1–3.9 ppm region (G). N—H shifts from primary amines (–NH_2) perceived at 6.9–6.7 ppm (F) are ascribed to the reaction of MDI with residual water (Delebecq et al., 2013; Wicks & Wicks, 1999). The primary amine formed reacts with free NCO groups generating disubstituted ureas, whose N—H resonance is identified at 8.5 ppm (C). A peak at 10.1 ppm (A) due to the N—H of allophanates is also observed (Yang et al., 2014). Fig. 2(b) and (c) show possible paths for di-substituted urea and allophanate formation. Peak A at 10.1 ppm is due to allophanates and peak B at 9.3 ppm is attributed to phenyl carbamate. Peak C at 8.5 ppm is ascribed to disubstituted urea, peak D at 7.4–7.3 ppm is due to aromatic rings from phenol, peak E at 7.1 ppm is attributed to aromatic rings from MDI, peak F at 6.9–6.7 ppm is due to primary amines, and peak G at 4.1–3.9 ppm is ascribed to methylene groups from MDI.

3.2. Characterization of films

Fig. 3.(a) displays the FTIR spectra of NFC films and the films modified with MDI-2Ph (NFC-MDI) and TMP-TDI-3Ph (NFC-TMP-TDI). NFC-MDI shows absorptions at 1716 cm^{-1}, 1598 cm^{-1}, 1542 cm^{-1}, 1510 cm^{-1}, and 1230 cm^{-1}, which are not present in the neat NFC film spectrum. The vibration at 1716 cm^{-1} is due to the C = O group of urethane formed with cellulose hydroxyl groups, whereas the phenyl-urethane of the blocked isocyanate (pH-MDI-pH spectra) occurs at 1720 cm^{-1}. The absorption at 1542 cm^{-1} due to the C—N urethane group also confirms the new urethane bonds formed and the absorption band at 1230 cm^{-1} in the NFC-MDI spectrum suggests the presence of secondary amides, as observed in the pH-MDI-pH spectrum.

Fig. 3.(b) shows the spectra of NFC, NFC-TMP-TDI, and TMP-TDI-3Ph The C = O stretching from the phenyl urethane band for the commercial blocked isocyanate appears at 1707 cm^{-1} and is shifted to 1720 cm^{-1} due to the reaction of free NCO and surface hydroxyls. The H—NCO vibration at 1600 cm^{-1} and the band of secondary amides at 1230 cm^{-1} are observed in the modified spectra, also confirming the new urethane bonds in the NFC-TMP-TDI structure.

The elemental analysis of NFC and modified NFC revealed 41.82% of carbon, 6.39% of hydrogen, and 0.29% of nitrogen for non-modified NFC, 43.13% of carbon, 6.06% of hydrogen, and 0.57% of nitrogen for NFC-MDI, and 43.26% of carbon, 6.01% of hydrogen, and 1.42% of nitrogen for NFC-TMP-TDI. The nitrogen content of non-modified NFC was used as blank.

NFC-TMP-TDI shows almost three times the amount of nitrogen found in the NFC-MDI structure, suggesting more density of urethane bonds, hence contributing to a stiffer and more compact structure. The amount of hydroxyl groups of cellulose available for a chemical modification on the NFC surface was calculated from the data of elemental analysis for nitrogen estimated from the amount of nitrogen in the compound. The nitrogen content found in NFC as used as the blank value and its value was decreased from the values for the NFC-MDI and NFC-TMP-TDI giving respectively 0.28% and 1.13% of nitrogen for these compounds. The data enabled the estimation of the accessible hydroxyl groups content at approximately 1% from the total in the NFC, which is in accordance with that obtained for cellulose pulp in Gironès et al., (2008).

Fig. 4 depicts the solid state ^{13}C NMR spectra of NFC-MDI and NFC-TMP-TDI films. Peaks ascribed as 1to 6 refer to the cellulose backbone and were detected in both modified films, indicating the maintenance of their primary structures. Resonances at 154.5 ppm (A), related to C=O groups from urethanes, and at137–130 ppm (B), due to C—C bonds from aromatic rings of TDI and MDI, respectively, are evidences of chemical reactions during the de-blocking step of MDI-2Ph and TMP-TDI-3Ph

Fig. 5 shows photographs of pristine (a) and films modified with MDI (b) and TMP-TDI (c), respectively. The pristine film is translucent, whereas NFC-MDI and NFC-TMP-TDI are more opaque, with an amber coloration as observed by visual inspection. The light transmission values on T_{660nm} are provided at the bottom of each image, confirming the modified films supply a lower percentage of light transmittance in comparison with the base NFC film and their opaqueness is related to the optical haze effect (Tsalagkas et al., 2017)). As shown in the UV-VIS spectra in the supplementary material, Fig. S1, NFC-MDI absorbs light in the range of UVB and UVA. NFC-TMP-TDI absorbs UVA, UVB, and violet and blue wavelengths, whereas non- modified NFC shows a lower light absorption in the range of UV and visible wavelengths. Similar results were obtained by Chen et al., (2021) with the incorporation of Cu-Metal organic frameworks in cellulose acetate films.

Concerning the surface of the films, roughness (Rq) data are provided in the supplementary materials, Table S2, and SEM surface images are shown in Fig. S2. The roughnesses of modified films are similar, but higher than that of the non-modified one. According to MEV, all materials display similar morphologies. The cross-section SEM images show a very compacted, layered, and homogeneous section for the three compositions. In general, a spaced layered section is typical of NFC and cross-linked NFC films (Djafari Petroudy et al., 2019; Lossada et al., 2019; Sethi et al., 2019, 2018; Solala et al., 2018). The films obtained here seem slightly more compacted than those reported in the literature.

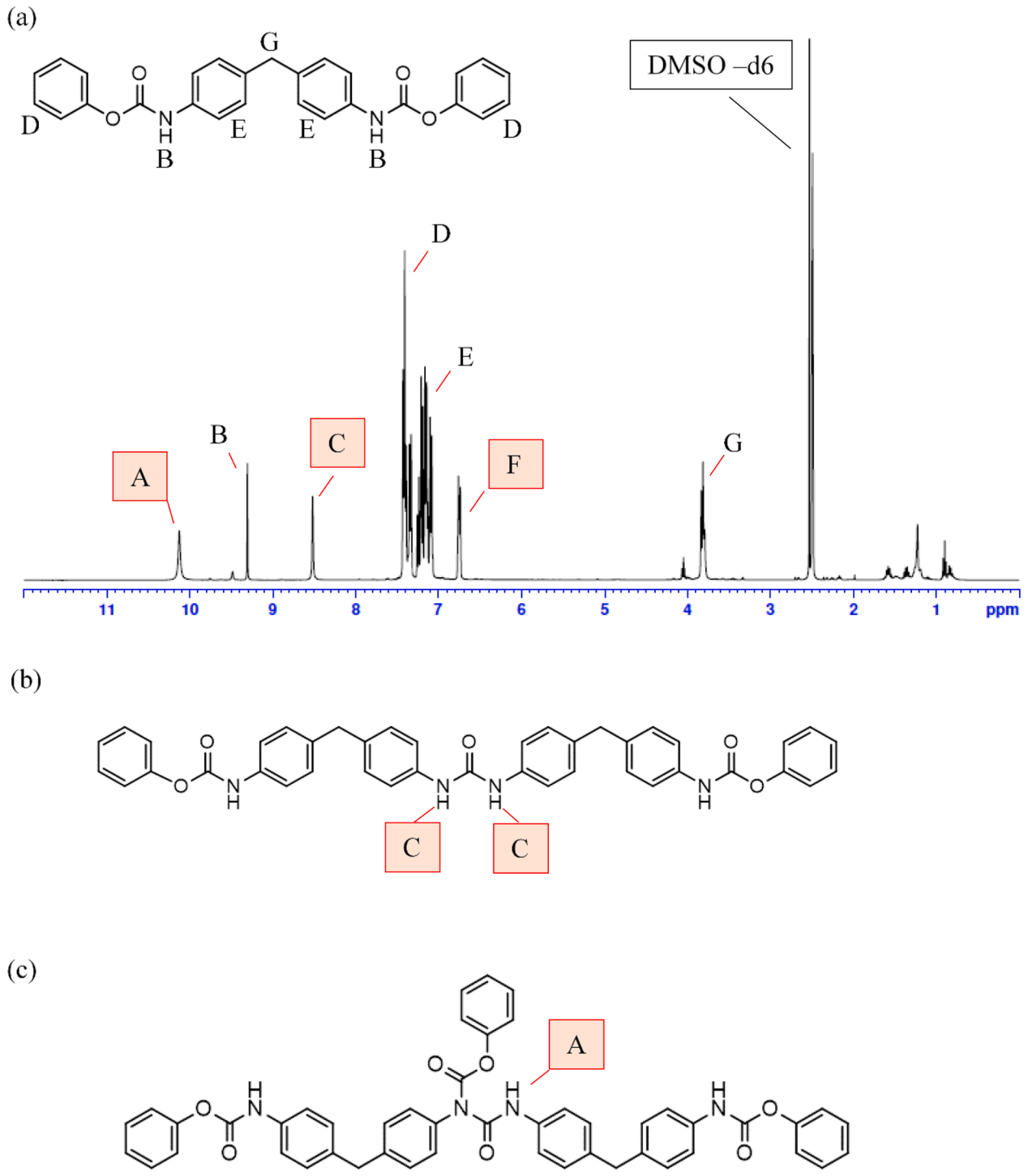

Fig. 2. (a)^{1}H NMR spectrum of synthetized pH-MDI-pH blocked diisocyanate in DMSO-d6. Possible path for (b) disubstituted ureas and (c) allophanates formation due to the reaction of a partially blocked phenol-MDI with a second MDI molecule.

Table S3shows data on thickness, grammage, density, and porosity of the films - modified films are thicker and show higher grammage due to the presence of chemicals. Nonetheless, density and porosity are in the same range of pristine NFC, i.e., near 1.1 g cm^{-3} and 25%, respectively.

Table 1 shows data on Young's modulus, tensile strength (TS), strain at break, and work of fracture (WOF) of the films along with its correspondent statistical group. The statistical group, obtained through the Tukey's analysis with 95% of confidence, is represented by the letters (a, b, or c) in which the subscription simply identify the property analyzed on the group, for example a' is from Tensile Strength and a$^{\#}$ is from tear index. Tensile stress vs strain curves are provided in Fig. S3 in the supplementary material. The chemical modification of NFC causes a moderate decrease in modulus (group a for NFC and group b for NFC-MDI and NFC-TMP-TDI) and a large decrease in tensile strain and work of fracture. The value for Young modulus observed for the modified films is higher than those of other polyurethane biobased composites recently described for packaging (Kim et al., 2021; Urbina et al., 2019). The reduction in modulus and tensile strength of modified films in relation to pristine films may be a result of the formation of a urethane layer around fibers, whose interaction is weaker than the fiber-to-fiber

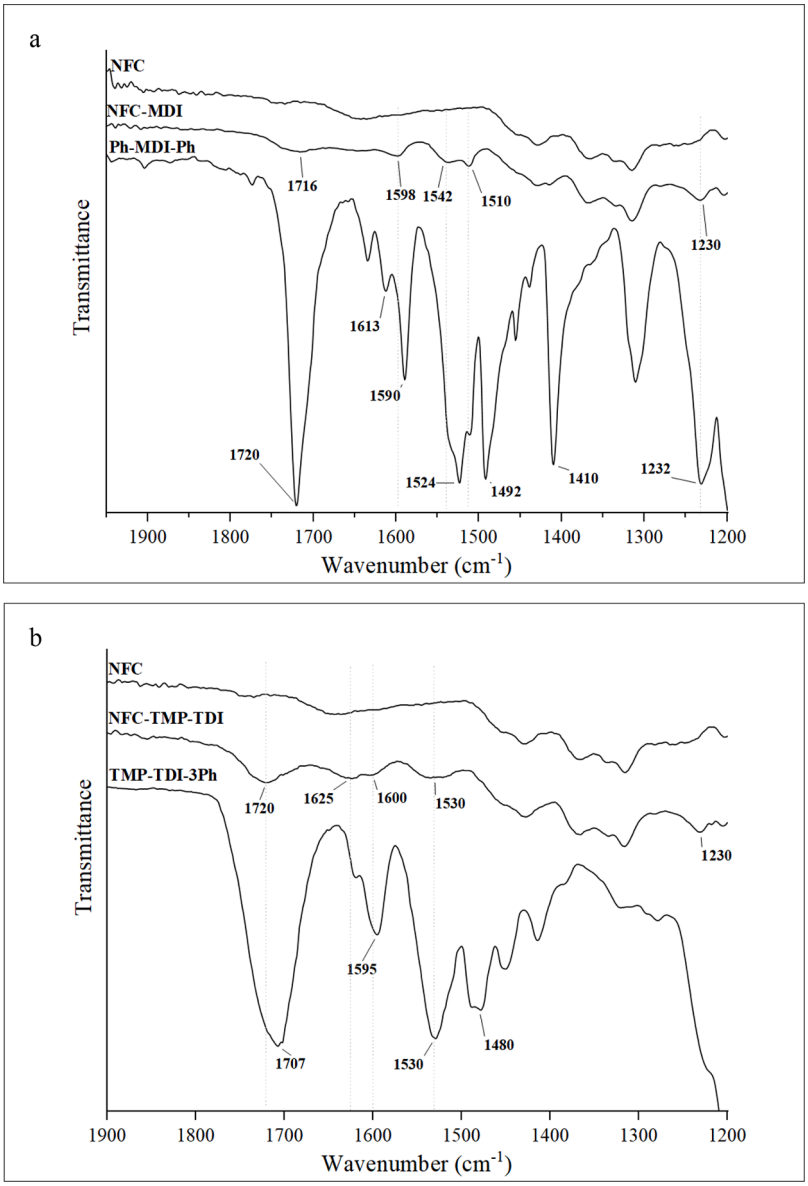

Fig. 3. ATR-FTIR spectra of (a) NFC-MDI and pH-MDI-pH and (b) NFC-TMP-TDI and TMP-TDI-3Ph modified films. Neat NFC films are displayed in both spectra.

one. Tear test indexes for NFC-MDI and NFC-TMP-TDI are slight higher than that of modified NFC.

Table 2 depicts the wet tensile properties conditions Despite its highest tensile properties in the dry state, NFC film was the most affected by the contact with water, showing approximately 90% of reduction in its Young modulus, although the ratio for TS and strain at break remained high. NFC-MDI presented modulus value almost identical to its dry property whereas NFC-TMP-TDI showed a little decrease, evidenced by the alteration of the statistic group, showing the chemical modifications successfully reduced or even inhibited the water plasticizing effect.

The profiles of thermogravimetric losses for NFC, NFC-MDI, and NFC-TMP-TDI are similar, with an onset of thermal degradation at approximately 280 °C and a large decay of more than 60% up to 406 °C. NFC shows another gradual decay starting at 406 °C, with total decomposition of carbon matter until 700 °C, whereas NFC-MDI and NFC-TMP-TDI display a less pronounced loss with 20–30% of residual material (curves are shown in Fig. S4 in the supplementary material)

The water vapor uptake was not affected by the chemical treatment and was lower than 10% (the curves of water vapor absorption as a function of time are shown in supplementary materials, Fig. S5).

The chemical treatment with pH-MDI-pH led to an 86% increase in the water contact angle (WCA),whereas the treatment with TMP-TDI-3Ph did not alter the WCA of the surface of the film, which was maintained at 52° (supplementary material, Fig. S6).

NFC film shows 87 ± 5 mN/m surface tension and NFC-MDI and NFC-TMP-TDI show surface tensions of 44 ± 9 mN/m and 72 ± 3 mN/m, respectively.

3.3. Barrier properties to water vapor and oxygen

Fig. 6 displays the mass increase (g) as a function of time (h) obtained in the WVTR test. Data on the permeation tests are shown in Table S3 in supplementary material.

Both treatments (NFC-MDI and NFC-TMP-TDI) effectively increased the barrier to water vapor, with approximately 74% reduction in WVTR with respect to the NFC film. The WVTR values around 40 g m^{-2}.day^{-1} of the modified films are well below some recently reported ones for biobased packaging (e.g.,PVA/lignin nanoparticles (Zhang et al., 2020), alginate/copper sulfide nanoparticles (Roy & Rhim, 2020),

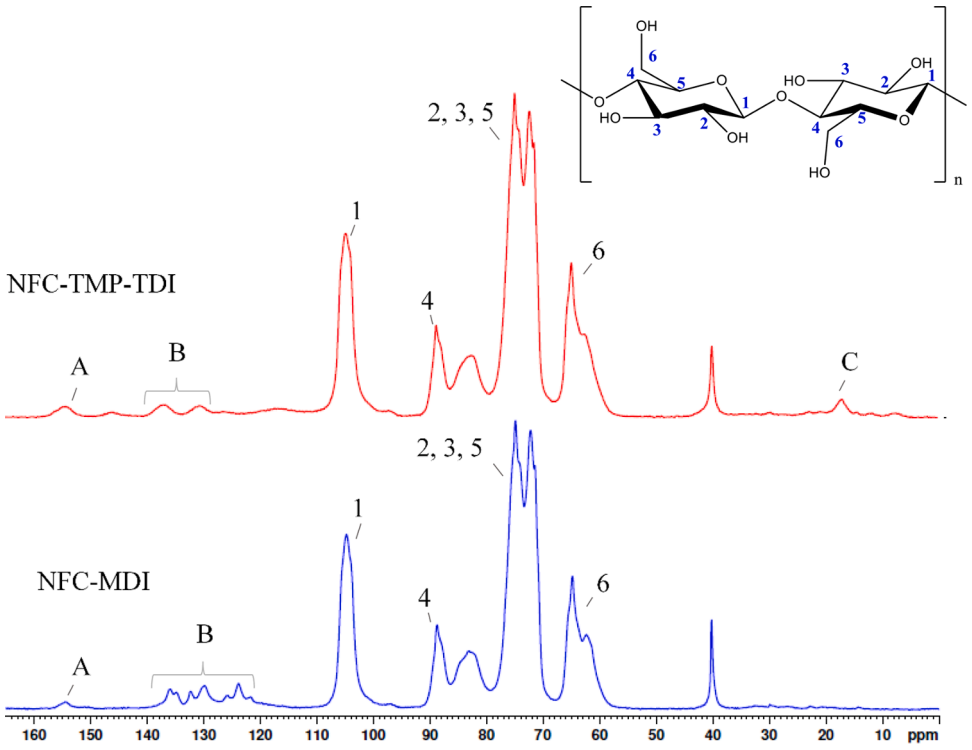

Fig. 4. (a) ATR-FTIR spectra and (b) ^{13}C NMR (solid) spectra of NFC-TMP TDI and NFC-MDI chemically modified films.

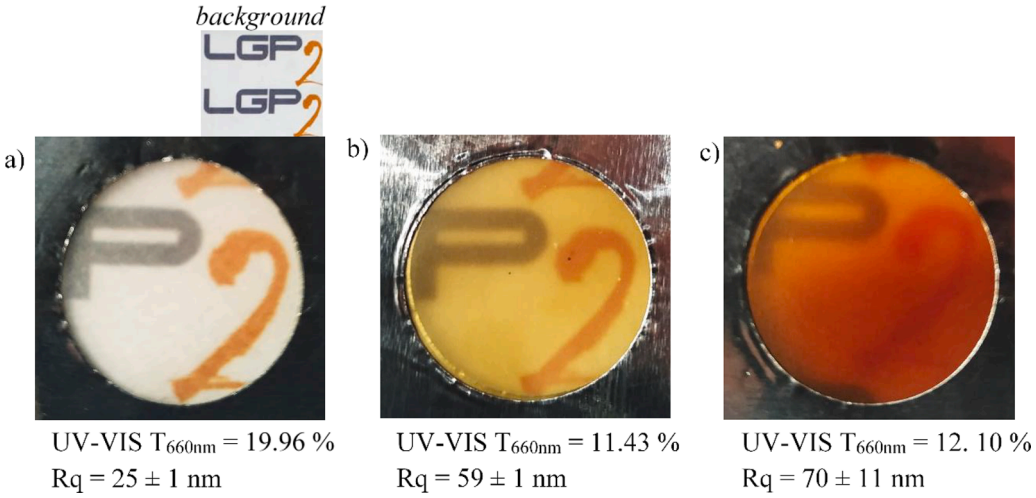

Fig. 5. Photographs of NFC film (a) and modified NFC-MDI (b) and NFC-TMP-TDI (c) counterparts. Rq are from AFM measurements. The edge length of the photos corresponds to 2 cm.

Table 1
Mechanical properties obtained from tensile and tear testings and tear test index.

Materials	Young's Modulus (GPa)	SG*	Tensile Strength (MPa)	SG*	Strain at Break (%)	SG*	Work to Fracture (MJ/m^3)	Tear testing index (mN*m^2/g) SG*		SG*
NFC	6.5 ± 0.7	a	108 ± 10	a'	9 ± 1	a''	8.0 ± 1.0	a'''	0.7 ± 0.1	b$^{\#}$
NFC-MDI	5.2 ± 0.3	b	62 ± 11	b'	2 ± 1	b''	1.2 ± 0.6	b'''	1.3 ± 0.4	a$^{\#}$
NFC-TMP-TDI	5.0 ± 0.1	b	73 ± 3	b'	3 ± 1	c''	1.4 ± 0.6	b'''	1.0 ± 0.2	a,b$^{\#}$

* SG = Statistic Group of Tukey's analysis at 95% confidence. The indices a b and c denote the groups of mean values and the subscription is related to the property analyzed.

lignocellulose nanopapers (Djafari Petroudy et al., 2019), and NFC/alkaili lignin composite (Wang et al., 2021)), which reached 60 g m^{-2}. day^{-1} in NFC/alkyl lignin composites.

Table 3 shows Water Vapor Permeability (WVP) values, of which that of pristine NFC can be considered low (J. Wang et al., 2018). However, the chemical modification with blocked diisocyanates

Table 2
Mechanical properties obtained from wet tensile test.

Materials	Young's Modulus (GPa)	SG*	Tensile Strength (MPa)	SG*	Strain at Break (%)	SG*	Work to Fracture (MJ/m^3)	SG*
NFC	0.8 ± 0.4	a	85 ± 8	a'	10 ± 2	a''	5 ± 1	a'''
NFC-MDI	4.9 ± 1.0	b	66 ± 6	b'	4 ± 1	b''	1.9 ± 0.7	b'''
NFC-TMP-TDI	4.0 ± 0.4	c	47 ± 8	c'	2 ± 1	b''	0.5 ± 0.2	c''

reduced the WVP by almost half, yielding values for water vapor barrier similar to those of PA6 and PLA.

Table 3 shows data for Fickian flux (J), Diffusion coefficient (Deff), and diffusion coefficient (Da). The order of magnitude (10^{-8} cm s^{-1}) for Da is in the range of the values for other compositions of NFC films (Rahmani Seraji et al., 2017). Da was reduced by half due to the chemical modification with different adducts. The equation proposed by Hu et al.,(Hu et al., 2019) calculated the path lengths, shown in Table 2. Since the modified films were thicker than NFC, the path length was naturally increased, also contributing to the reduction in water vapor permeation.

Flux (J) data and the equations of cylindrical pore model(Hou et al., 2019) provided 0.6–0.95 nm values of mean porous radius (Rf) (Table S4). Rf is more than one order higher than the required mean porous radius of 0.03 nm for Knudsen to be assumed as the main diffusion mechanism; therefore, the flux is mainly Fickian.

Table 3 also shows the values of Oxygen Transmission Rate (OTR) in cm^3 m^{-2}.day^{-1} for pristine and modified films at 0% RH. The OTR value of NFC is 15 ± 3 cm^3 m^{-2}.day^{-1}, which is suitable for its applications as a modified atmosphere packaging film. The OTR of NFC-MDI, modified with bifunctional bridging moieties (MDI-2Ph) is the same as that of untreated NFC films, indicating the chemical modification apparently exerted no effect on the oxygen transport in the structure of the film. On the other hand, the OTR of NFC-TMP-TDI, modified with trifunctional moiety (TMP-TDI-3Ph), is almost zero, i.e., below the detection limits of the equipment, probably due to the denser urethane bonds formed (Scheme S1).

3.4. Chemical modification with blocked isocyanates: summary of properties and structure prediction

According to the results of wet tensile tests, WVTR, and OTR, a chemical modification with MDI-2Ph and TMP-TDI-3Ph produces water-resistant and low permeable nanocellulose films. Fig. (a) and 7(b) show possible pathways for those reaction mechanisms with (MDI-2Ph) and the commercial trifunctional blocked isocyanate agent (TMP-TDI-3Ph), respectively. TMP-TDI-3Ph is a polyisocyanate with at least three isocyanate groups and higher molar mass with respect to MDI-2Ph, which facilitate the formation of carbamate bridges and lead to a crosslinked material with a higher urethane content. Nonetheless, the short chain length of MD-2Ph in relation to the size of the fibers was not as effective as that of TMP-TDI-3Ph in creating a chemical connection among the fibers, since it hampered the water passage; however, it was inefficient against oxygen transport.

4. Conclusions

Films of nanofibrilated cellulose (NFC) were obtained by casting a

Table 3
Data of Fickian diffusion parameters calculated with data from wet-cup permeance test of WVTR and WVP from wet-cup experiments, free path length, and OTR.

Fickian diffusion data	W (g/h)	w (mol/s)	J (mol cm^{-2}*s)	H (cm)	Deff (cm^2.s-1)
NFC	0.0191	2.95E-07	9.83E-09	0.0046	8.01E-09
NFC-MDI	0.0058	8.02E-08	2.67E-09	0.0093	4.41E-09
NFC-TMP-TDI	0.0052	8.95E-08	2.98E-09	0.0082	4.34E-09
WVPR	WVTR (g/(m^2*day))	WVP (g*μm/(m^2*day*kPa))	Da (cm^2 s^{-1})	Path length (μm)	OTR (cm^3 m^{-2}.day^{-1})
NFC	152.82	5065	6,19E-08	81.66	15±3
NFC-MDI	41.61	2788	2,96E-08	168.31	15±1
NFC-TMP-TDI	46.41	2742	2,83E-08	149.80	0.2 ± 0.2

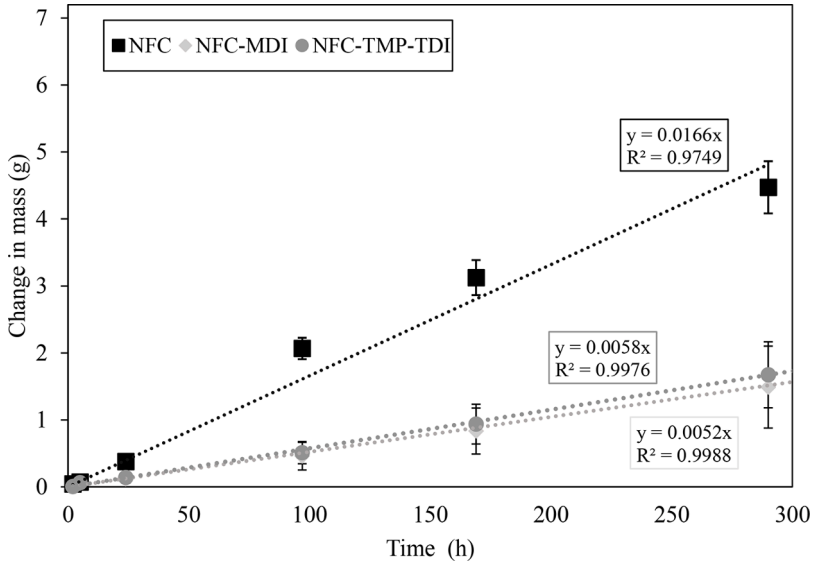

Fig. 6. Water mass increase as a function of time for pristine and modified films obtained by the wet cup permeance test.

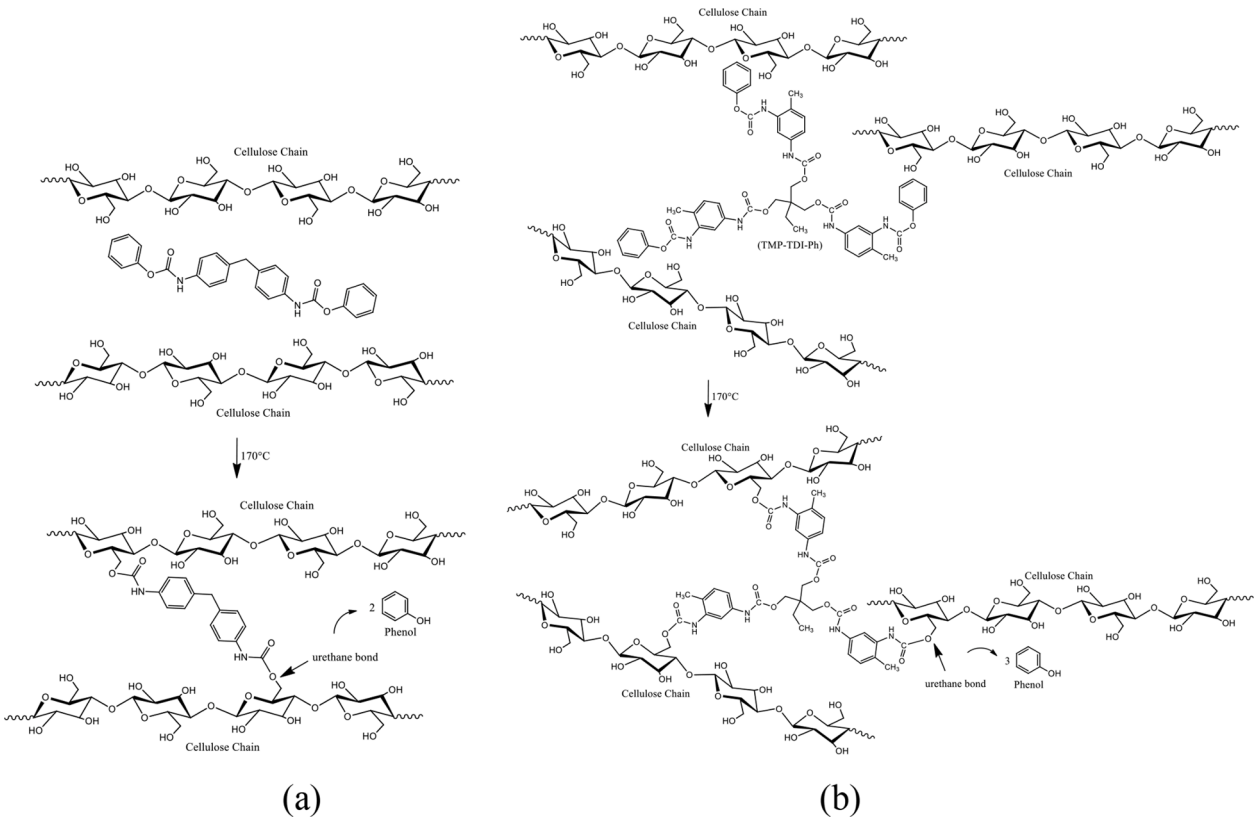

Fig. 7. (a) Possible pathway for NFC films crosslinking after thermal treatment with bifunctional adduct pH-MDI-pH and (b) Possible pathway for NFC films crosslinking after thermal treatment with trifunctional adduct TMP-TDI-3Ph

mixture of NFC aqueous suspensions with an emulsion of bi and trifunctional blocked isocyanates followed by a thermal treatment. The coupling urethane-NFC reaction was confirmed by FT-IR, EA and solid ^{13}C NMR. Tensile tests revealed the modified films maintained their mechanical properties unchanged when in contact with water, whereas that of pristine NFC shows, for example, a reduction of almost 90% in modulus. The water vapor transmission rate (WVTR) of modified films was reduced in comparison to their pristine precursor and the modification with trifunctional blocked isocyanate decreased the oxygen transmission rate (OTR) of the film. Although NFC films are good candidates to replace synthetic polymers in packaging films, their mechanical and barrier properties are highly affected by the humidity of the environment, thus requiring improvements in water resistance towards a wider range of applications. The results show the strategy proposed can efficiently maintain the mechanical and barrier properties of NFC films even in wet environments.

Funding

The authors also declare the **funding of this work.** This work was supported by Coordenação de Aperfeiçoamento de Pessoal de Nível Superior - Brasil (CAPES) – Grant number: Finance Code 001 and CNPq for the doctoral fellowship grant number CNPq proc. 140249/2017-6 both to GS and financial support to AJFC from CNPq for research funding project Grant number 03847/2019-0.

Supplementary materials

Supplementary materials associated with this article can be found in the online version, at doi.xxx.

CRediT authorship contribution statement

Gustavo de Souza: Conceptualization, Data curation, Formal analysis, Investigation, Methodology, Writing – original draft, Writing – review & editing. **Mohamed Naceur Belgacem:** Conceptualization, Supervision, Writing – review & editing. **Alessandro Gandini:** Conceptualization, Supervision, Writing – review & editing. **Antonio José Felix Carvalho:** Conceptualization, Data curation, Funding acquisition, Methodology, Project administration, Resources, Writing – review & editing.

Declaration of Competing Interest

The authors declare no competing financial interest. The authors declare that are not financial interests involving companies or other third parts. The authors also declare no conflict of interest of other kind.

Acknowledgements

This study was partially financed by the Coordenação de Aperfeiçoamento de Pessoal de Nível Superior - Brazil (CAPES) - Finance Code 001. The authors acknowledge CNPq for the doctoral fellowship granted to G.S (CNPq proc. 140249/2017–6), and Suzano S/A, Brazil, which kindly supplied the NFC from eucalyptus wood pulp. AJFC is indebted to CNPq for research funding project # 303847/2019–0. The authors also acknowledge Angela C.P. Giampedro from Centro Cultural - PUSP/SC for revising the manuscript.

Supplementary materials

Supplementary material associated with this article can be found, in the online version, at doi:10.1016/j.carpta.2022.100249.

References

Balu, B., Breedveld, V., & Hess, D. W. (2008). Fabrication of "roll-off" and "sticky" superhydrophobic cellulose surfaces-via plasma processing. *Langmuir : the ACS journal of surfaces and colloids, 24*(9), 4785–4790. https://doi.org/10.1021/la703766c

Carvalho, A. J. F., Curvelo, A. A. S., & Gandini, A. (2005). Surface chemical modification of thermoplastic starch: Reactions with isocyanates, epoxy functions and stearoyl chloride. *Industrial Crops and Products, 21*(3), 331–336. https://doi.org/10.1016/j.indcrop.2004.04.027

Chen, K., Yu, J., Huang, J., Tang, Q., Li, H., & Zou, Z. (2021). Improved mechanical, water vapor barrier and UV-shielding properties of cellulose acetate films with flower-like metal-organic framework nanoparticles. *International Journal of Biological Macromolecules, 167*, 1–9. https://doi.org/10.1016/j.ijbiomac.2020.11.164

de Souza, G., Belgacem, M. N., Gandini, A., & Carvalho, A. J. F. (2021). Low permeable hydrophobic nanofibrilated cellulose films modified by dipping and heating processing technique. *Cellulose (London, England), 28*(3), 1617–1632. https://doi.org/10.1007/s10570-020-03619-3

Delebecq, E., Pascault, J. P., Boutevin, B., & Ganachaud, F. (2013). On the versatility of urethane/urea bonds: Reversibility, blocked isocyanate, and non-isocyanate polyurethane. *Chemical Reviews, 113*(1), 80–118. https://doi.org/10.1021/cr300195n

Djafari Petroudy, S. R., Rahmani, N., Rasooly Garmaroody, E., Rudi, H., & Ramezani, O. (2019). Comparative study of cellulose and lignocellulose nanopapers prepared from hard wood pulps: Morphological, structural and barrier properties. *International Journal of Biological Macromolecules, 135*, 512–520. https://doi.org/10.1016/j.ijbiomac.2019.05.212

Forsman, N., Lozhechnikova, A., Khakalo, A., Johansson, L. S., Vartiainen, J., & Österberg, M. (2017). Layer-by-layer assembled hydrophobic coatings for cellulose nanofibril films and textiles, made of polylysine and natural wax particles. *Carbohydrate Polymers, 173*, 392–402. https://doi.org/10.1016/j.carbpol.2017.06.007

Gandini, A., & Belgacem, M.N. (.2016). The Surface and In-Depth Modification of Cellulose Fibers. In O. J. Rojas (Ed.), *Cellulose chemistry and properties: Fibers, nanocelluloses and advanced materials* (pp. 169–206). Springer International Publishing. https://doi.org/10.1007/12_2015_305.

Ghasemlou, M., Daver, F., Ivanova, E. P., Habibi, Y., & Adhikari, B. (2021). Surface modifications of nanocellulose: From synthesis to high-performance nanocomposites. *Progress in Polymer Science, 119*, Article 101418. https://doi.org/10.1016/J.PROGPOLYMSCI.2021.101418

Gironès, J., Pimenta, M. T. B., Vilaseca, F., Carvalho, A. J. F., Mutjé, P., & Curvelo, A. A. S. (2008). Blocked diisocyanates as reactive coupling agents: Application to pine fiber-polypropylene composites. *Carbohydrate Polymers, 74*(1), 106–113. https://doi.org/10.1016/j.carbpol.2008.01.026

Gironès, J., Pimenta, M. T. B., Vilaseca, F., de Carvalho, A. J. F., Mutjé, P., & Curvelo, A. A. S. (2007). Blocked isocyanates as coupling agents for cellulose-based composites. *Carbohydrate Polymers, 68*(3), 537–543. https://doi.org/10.1016/j.carbpol.2006.10.020

González, I., Alcalà, M., Chinga-Carrasco, G., Vilaseca, F., Boufi, S., & Mutjé, P. (2014). From paper to nanopaper: Evolution of mechanical and physical properties. *Cellulose (London, England), 21*(4), 2599–2609. https://doi.org/10.1007/s10570-014-0341-0

Habibi, Y. (2014). Key advances in the chemical modification of nanocelluloses. *Chemical Society Reviews, 43*(5), 1519–1542. https://doi.org/10.1039/c3cs60204d

Hou, T., Guo, K., Wang, Z., Zhang, X. F., Feng, Y., He, M., et al. (2019). Glutaraldehyde and polyvinyl alcohol crosslinked cellulose membranes for efficient methyl orange and Congo red removal. *Cellulose (London, England), 26*(8), 5065–5074. https://doi.org/10.1007/s10570-019-02433-w

Hu, Y., Acharya, S., & Abidi, N. (2019). Cellulose porosity improves its dissolution by facilitating solvent diffusion. *International Journal of Biological Macromolecules, 123*, 1289–1296. https://doi.org/10.1016/j.ijbiomac.2018.10.062

Hubbe, M. A., Gardner, D. J., & Shen, W. (2015). Wettability of cellulosics. *Bioresources, 10*(4), 8657–8749. https://pdfs.semanticscholar.org/5abd/c6f4c89c252cc44f20d584f9db06444c3e52.pdf.

Kim, M. S., Ryu, K. M., Lee, S. H., Choi, Y. C., Rho, S., & Jeong, Y. G. (2021). Chitin Nanofiber-Reinforced Waterborne Polyurethane Nanocomposite Films with Enhanced Thermal and Mechanical Performance. *Carbohydrate Polymers, 258* (January), Article 117728. https://doi.org/10.1016/j.carbpol.2021.117728

Klemm, D., Cranston, E. D., Fischer, D., Gama, M., Kedzior, S. A., Kralisch, D., et al. (2018). Nanocellulose as a natural source for groundbreaking applications in materials science: Today's state. *Materials Today, 21*(7), 720–748. https://doi.org/10.1016/j.mattod.2018.02.001

Lindström, T., & Aulin, C. (2014). Market and technical challenges and opportunities in the area of innovative new materials and composites based on nanocellulosics. *Scandinavian Journal of Forest Research, 29*(4), 345–351. https://doi.org/10.1080/02827581.2014.928365

Lossada, F., Guo, J., Jiao, D., Groeer, S., Bourgeat-Lami, E., Montarnal, D., et al. (2019). Vitrimer Chemistry Meets Cellulose Nanofibrils: Bioinspired Nanopapers with High Water Resistance and Strong Adhesion [Research-article]. *Biomacromolecules, 20*(2), 1045–1055. https://doi.org/10.1021/acs.biomac.8b01659

Lu, Z., Huang, J., E, S., Li, J., Si, L., Yao, C., et al. (2020). All cellulose composites prepared by hydroxyethyl cellulose and cellulose nanocrystals through the crosslink of polyisocyanate. *Carbohydrate Polymers, 250*(August), Article 116919. https://doi.org/10.1016/j.carbpol.2020.116919

Mahmud, S., Hasan, K. M. F., Jahid, M. A., Mohiuddin, K., Zhang, R., & Zhu, J. (2021). Comprehensive review on plant fiber-reinforced polymeric biocomposites. In *Journal of Materials Science, 56*(12), 7231–7264. https://doi.org/10.1007/s10853-021-05774-9. Springer US.

Nechyporchuk, O., Belgacem, M. N., & Bras, J. (2016). Production of cellulose nanofibrils: A review of recent advances. *Industrial Crops and Products, 93*, 2–25. https://doi.org/10.1016/j.indcrop.2016.02.016

Operamolla, A. (2019). Recent advances on renewable and biodegradable cellulose nanopaper substrates for transparent light-harvesting devices: Interaction with humid environment. *International Journal of Photoenergy, 2019*, 1–16. https://doi.org/10.1155/2019/3057929.

Paquet, O., Krouit, M., Bras, J., Thielemans, W., & Belgacem, M. N. (2010). Surface modification of cellulose by PCL grafts. *Acta Materialia, 58*(3), 792–801. https://doi.org/10.1016/j.actamat.2009.09.057

Rahmani Seraji, H., Karimi, M., & Mahmoudi, L. (2017). In situ monitoring the change of mechanical response induced by the diffusion of saline water in glassy cellulose acetate. *Desalination, 420*(July), 191–207. https://doi.org/10.1016/j.desal.2017.07.013

Rol, F., Belgacem, M. N., Gandini, A., & Bras, J. (2019). Recent advances in surface-modified cellulose nanofibrils. *Progress in Polymer Science, 88*, 241–264. https://doi.org/10.1016/j.progpolymsci.2018.09.002

Roy, S., & Rhim, J. W. (2020). Effect of CuS reinforcement on the mechanical, water vapor barrier, UV-light barrier, and antibacterial properties of alginate-based composite films. *International Journal of Biological Macromolecules, 164*, 37–44. https://doi.org/10.1016/j.ijbiomac.2020.07.092

Sehaqui, H., Zimmermann, T., & Tingaut, P. (2014). Hydrophobic cellulose nanopaper through a mild esterification procedure. *Cellulose (London, England), 21*(1), 367–382. https://doi.org/10.1007/s10570-013-0110-5

Sethi, J., Farooq, M., Österberg, M., Illikainen, M., & Sirviö, J. A. (2018a). Stereoselectively water resistant hybrid nanopapers prepared by cellulose nanofibers and water-based polyurethane. *Carbohydrate Polymers, 199*(July), 286–293. https://doi.org/10.1016/j.carbpol.2018.07.028

Sethi, J., Farooq, M., Sain, S., Sain, M., Sirviö, J. A., Illikainen, M., et al. (2018b). Water resistant nanopapers prepared by lactic acid modified cellulose nanofibers. *Cellulose (London, England), 25*(1), 259–268. https://doi.org/10.1007/s10570-017-1540-2

Sethi, J., Visanko, M., Österberg, M., & Sirviö, J. A. (2019). A fast method to prepare mechanically strong and water resistant lignocellulosic nanopapers. *Carbohydrate Polymers, 203*(September 2018), 148–156. https://doi.org/10.1016/j.carbpol.2018.09.037

Siqueira, G., Bras, J., & Dufresne, A. (2010). Cellulosic bionanocomposites: A review of preparation, properties and applications. *Polymers, 2*(4), 728–765. https://doi.org/10.3390/polym2040728

Solala, I., Bordes, R., & Larsson, A. (2018). Water vapor mass transport across nanofibrillated cellulose films: Effect of surface hydrophobization. *Cellulose (London, England), 25*(1), 347–356. https://doi.org/10.1007/s10570-017-1608-z

Sugiarto, S., Pong, R. R., Tan, Y. C., Leow, Y., Sathasivam, T., Zhu, Q., et al. (2022). Advances in sustainable polymeric materials from lignocellulosic biomass. *Materials Today Chemistry, 26*, Article 101022. https://doi.org/10.1016/J.MTCHEM.2022.101022

Tsalagkas, D., Zhai, L., Kim, H. C., & Kim, J. (2017). Optical and mechanical properties of cellulose nanopaper structures. *Nanosensors, Biosensors, Info-Tech Sensors and 3D Systems 2017, 10167*(April 2017), Article 101670E. https://doi.org/10.1117/12.2259839

Urbina, L., Corcuera, M.Á., Eceiza, A., & Retegi, A. (2019). Stiff all-bacterial cellulose nanopaper with enhanced mechanical and barrier properties. *Materials Letters, 246*, 67–70. https://doi.org/10.1016/j.matlet.2019.03.005

Wang, J., Gardner, D. J., Stark, N. M., Bousfield, D. W., Tajvidi, M., & Cai, Z. (2018). Moisture and Oxygen Barrier Properties of Cellulose Nanomaterial-Based Films. *ACS Sustainable Chemistry & Engineering, 6*(1), 49–70. https://doi.org/10.1021/acssuschemeng.7b03523

Wang, W., Gu, F., Deng, Z., Zhu, Y., Zhu, J., Guo, T., et al. (2021). Multilayer surface construction for enhancing barrier properties of cellulose-based packaging. *Carbohydrate Polymers, 255*(November 2020), Article 117431. https://doi.org/10.1016/j.carbpol.2020.117431

Wicks, D.a., & Wicks, Z. W. (1999). Blocked isocyanates III: Part A. Mechanisms and chemistry. *Progress in Organic Coatings, 36*(3), 148–172. https://doi.org/10.1016/S0300-9440(99)00042-9

Yang, R., Wang, Y., & Li, M. (2014). Homogeneous synthesis of crosslinked cellulose spheres from hemp (Cannabis sativa L.) stem and cotton. *Cellulose Chemistry and Technology, 48*(5–6), 455–459.

Zhang, X., Liu, W., Liu, W., & Qiu, X. (2020). High performance PVA/lignin nanocomposite films with excellent water vapor barrier and UV-shielding properties. *International Journal of Biological Macromolecules, 142*, 551–558. https://doi.org/10.1016/j.ijbiomac.2019.09.129

Zhou, X., Fu, Y., Chen, L., Wang, R., Wang, X., Miao, Y., et al. (2020). Diisocyanate modifiable commercial filter paper with tunable hydrophobicity, enhanced wet tensile strength and antibacterial activity. *Carbohydrate Polymers, 248*(July), Article 116791. https://doi.org/10.1016/j.carbpol.2020.116791